Acta Biomaterialia 158 (2023) 281–291

Contents lists available at ScienceDirect

Acta Biomaterialia

journal homepage: www.elsevier.com/locate/actbio

Full length article

A micropatterned thermoplasmonic substrate for neuromodulation of *in vitro* neuronal networks

Andrea Andolfi[a], Pietro Arnaldi[a], Donatella Di Lisa[a], Sara Pepe[b], Monica Frega[c], Anna Fassio[b], Alberto Lagazzo[d], Sergio Martinoia[a], Laura Pastorino[a,*]

[a] Department of Informatics, Bioengineering, Robotics and Systems Engineering (DIBRIS), University of Genoa, Genoa, Italy
[b] Department of Experimental Medicine, University of Genoa, Genoa, Italy
[c] Department of Clinical Neurophysiology, University of Twente, Enschede, the Netherlands
[d] Department of Civil, Chemical and Environmental Engineering (DICCA), University of Genoa, Genoa, Italy

ARTICLE INFO

Article history:
Received 9 August 2022
Revised 5 December 2022
Accepted 15 December 2022
Available online 21 December 2022

Keywords:
Chitosan
Gold nanorods
Patterned neuronal networks
Thermoplasmonic effect
Neuronal stimulation

ABSTRACT

Understanding how the spatial organization of a neural network affects its activity represents a leading issue in neuroscience. Thanks to their accessibility and easy handling, *in vitro* studies remain an essential tool to investigate the relationship between the structure and function of a neuronal network. Among all the patterning techniques, ink-jet printing acquired great interest thanks to its direct-write approach, which allows the patterned substrate realization without mold, leading to a considerable saving of both cost and time. However, the inks commonly used give the possibility to control only the structure of a neuronal network, leaving aside the functional aspect. In this work, we synthesize a photosensitive ink combining the rheological and bioadhesive properties of chitosan with the plasmonic properties of gold nanorods, obtaining an ink able to control both the spatial organization of a two-dimensional neuronal network and its activity through photothermal effect. After the ink characterization, we demonstrate that it is possible to print, with high precision, different geometries on a microelectrode array. In this way, it is possible obtaining a patterned device to control the structure of a neuronal network, to record its activity and to modulate it via photothermal effect. Finally, to our knowledge, we report the first evidence of photothermal inhibition of human neurons activity.

Statement of significance

Patterned cell cultures remain the most efficient and simple tool for linking structural and functional studies, especially in the neuronal field. Ink-jet printing is the technique with which it is possible to realize patterned structures in the fastest, simple, versatile and low-cost way. However, the inks currently used permit the control only of the neuronal network structure but do not allow the control-modulation of the network activity. In this study, we realize and characterize a photosensitive bioink with which it is possible to drive both the structure and the activity of a neuronal network. Moreover, we report the first evidence of activity inhibition by the photothermal effect on human neurons as far as we know.

1. Introduction

The possibility of fabricating engineered platforms, able to reproduce aspects of the physiology of brain tissue, has attracted growing interest for the study of the mechanisms that regulate the central nervous system and in the study of neurodegenerative diseases [1,2]. Among all the numerous brain-on-a-chip models that have been developed over the years, the ones that allow the simultaneous stimulation and recording of electrophysiological activity by means of multielectrode arrays (MEAs) devices are of particular interest [3,4]. These platforms constitute an important resource for scale studies of network dynamics and high-throughput drug screening, by means of 2D neuronal cultures providing a simplified *in vitro* model with high parameter control [5–7]. The versatility of these systems, thanks to the large recording area, has made them essential in the study of the relationship between

* Corresponding author.
E-mail addresses: andrea.andolfi@edu.unige.it (A. Andolfi), pietro.arnaldi@dibris.unige.it (P. Arnaldi), donatella.dilisa@edu.unige.it (D.D. Lisa), sara.pepe@edu.unige.it (S. Pepe), m.frega@utwente.nl (M. Frega), anna.fassio@unige.it (A. Fassio), alberto.lagazzo@unige.it (A. Lagazzo), sergio.martinoia@unige.it (S. Martinoia), laura.pastorino@unige.it (L. Pastorino).

https://doi.org/10.1016/j.actbio.2022.12.036
1742-7061/

the functional activity of neuronal networks and their structural organization [3,8]. In this respect, different strategies have been adopted to fabricate culture supports with microscopic features that impose a defined adhesion pattern for neuronal cells [9,10]. To obtain engineered networks, different fabrication methods are possible, involving physical and/or chemical approaches to guide cell adhesion and growth. Technological developments in microfabrication, micro-deposition and micro-fluidics have allowed the application of methodologies such as UV photoablation [11], photothermal micro-fabrication [12], soft-lithography [13], photoresist patterning [14], photolithography [15], micro-machined substrates [16], micro-molding [17] and micro-contact printing [18,19]. Another patterning technique that has attracted great interest thanks to its low cost, scalability, non-invasiveness and versatility properties is ink-jet printing, which allows the localized deposition of ink micro-droplets without contacting the printing substrate [20]. Although the ink-jet printing of biomolecule has been proposed in the past [21], high-precision printing of aqueous solutions remains difficult, due to the problems associated with the surface tension of the used solutions [22].

Recently, we demonstrated that the cationic polysaccharide chitosan is by itself able to sustain neuronal adhesion and the maturation of both 2D and 3D functional neuronal networks [23–26]. Moreover, we demonstrated its printability [27]. In order to better understand the relationship between the structure and function of a neuronal network, in addition to the control of its spatial organization, the control of electrophysiological activity also becomes crucial [28–30]. Extracellular electrical stimulation of a neuronal network has been used in recent decades to study the dynamics and plasticity of a neuronal network [31]. However, even though reasonable temporal control is achieved, it is mainly intended for the excitation of nerve tissues to depolarize the cell membrane [32]. Although chemical stimulation is used both to excite and inhibit the activity of a neuronal network, it lacks the millisecond-scale precision that characterizes normal neural activity [32]. Thanks to the combination of optical stimulation and genetic modification, optogenetic in recent years has been proposed to excite and inhibit the activity of a neuronal network in a non-invasive way and with high space-time control [33]. However, despite the great promise, the difficult stability of gene expression has severely limited its use [34]. At the same time, an alternative for the inhibition of neuronal activity with high space-time control and without the need for any genetic modification has been realized exploiting the thermoplasmonic properties of gold nanorods (GNRs) [35–37].

Another important aspect to take into account in developing advanced *in vitro* neuronal models is represented by the neuronal cell source. The animal model remains the gold standard as well as an excellent tool for the study of neuropathologies *in vitro*, but for some significant species differences, it is not able to guarantee faithful reproduction of human pathophysiological conditions [38–40]. For this reason, even in the field of neuronal stimulation-modulation, *in vitro* studies are increasingly focusing on human models, specifically for electrical [41,42], piezoelectric [43], ultrasonic [44], optogenetic [45], and optical [46] stimulation, but still missing the thermoplasmonic ones.

The use of chitosan together with GNRs has been widely studied as a mean by which to improve the biocompatibility of metal nanoparticles for cancer therapy applications [47,48] and in tissue engineering applications [49,50].

In this work, we have combined the bioactive and rheological properties of chitosan with the thermoplasmonic properties of GNRs to obtain a photosensitive and printable ink to be used with a standard commercial piezoelectric printer. The developed ink has been then used to control the structure and the activity of neuronal cultures derived from rat embryos and from human induced pluripotent stem cells (iPSCs). To our knowledge, this is the first data reported in the literature of human neural activity inhibition by photothermal effect. Indeed, this localized photothermal stimulation technique stands as an alternative to that using uniform nanoparticle deposition and localized light stimulation, which, requires a digital micromirror device to localize the stimulation, surface functionalization to allow the nanoparticles to be anchored to the MEA substrate and then their functionalization with an adhesion factor [36].

This work aims to provide an easy, versatile, fast and low-cost tool for the study of the recurring relationship between the structure and function of neuronal networks.

2. Materials and methods

2.1. Materials

Low molecular weight chitosan (50–190 kDa, 77% deacetylation degree), glacial acetic acid, ethanol (EtOH), chloroauric acid (HAuCl4), Cetrimonium bromide (CTAB), Silver Nitrate (AgNO3), L-ascorbic acid and Sodium Borohydride (NaBH4) were purchased from Sigma-Aldrich.

2.2. Synthesis and characterization of gold nanorods (GNRs)

GNRs were synthesized by a seed-mediated method, following the protocol used by Yoo et al. [36]. The synthesized GNRs were purified by centrifugation at 12850 rcf for 10 min, and the pellet was resuspended in ultrapure water. The UV−vis extinction spectrum was measured using an UV–vis spectrophotometer (Cary 60, Agilent Technologies), while the size and morphology of GNRs were imaged using a Transmission Electron Microscope (TEM, Hitachi 7800, Japan) with Megaview G3 camera and EMSIS Radius 2.0 software (Muenster, Germany).

2.3. Preparation and characterization of CHI-GNRs composite ink

Different concentration of CHI (0.1%, 0.5% and 1% w/v) were dissolved in aqueous solutions of glacial acetic acid at different molarities (0.1, 0.5 and 1 M). CHI solutions were filtered with a syringe filter (0.5 µm pore size) to remove polymeric aggregates [25]. Viscosity and contact angle were evaluated to find the composition that best suits the printing parameters provided by the printer manufacturer. Rheometric measurements were performed with a modular compact rheometer (Physica MCR 301, Anton Paar), using a cone-plate (diameter = 50 mm, cone angle = 2°) at a constant temperature of 23 °C. Contact angle experiments were carried out on glass substrate (without any previous treatment) at room temperature by means of a home-made contact angle analyser, using the sessile drop method and the ImageJ software (NIH, "contact angle" plugin), to measure angles amplitude. To obtain a good data reliability, tests were repeated at least twice. Once the proper formulation was found, composite inks were obtained by adding concentrated GNRs to the chitosan solution and vortex for 2 min to get a stable colloidal dispersion. Different amount of concentrated GNRs were added to obtain different final concentrations expressed in terms of optical density (OD), specifically 2, 4 and 8 OD, 1 OD corresponding to $\sim$ 7.25 * 1011 GNRs/mL.

These formulations were subjected to the same rheometric characterizations described above and, in addition, to a UV-vis analysis to evaluate the ink optical properties.

2.4. Ink temperature measurement

The photothermal effect of the ink was evaluated in air conditions by depositing a drop of 20 µL of CHI-GNRs on the MEAs surface. The device was stimulated with a fiber-optic laser (785 nm,

450 mW, B&W Tek, USA), at a distance of less than 1 cm, and the laser beam from the bottom of the device formed a 5 mm diameter of illumination area on the MEA chip. The temperature change during NIR irradiation (3 min each) was measured using an infrared thermographic camera (TG165-X, FLIR, USA) and the samples were cooled down at RT before start the next measurement.

2.5. Patterns deposition process and characterization

Printing was carried out using a drop-on-demand (DOD) piezoelectric printer (Dimatix Materials Printer 2800 - DMP 2800 m,Fujifilm, Santa Clara, CA), equipped with a 16 nozzle and 10 pL cartridge (DMCLCP-11610). Printing parameters and patterns design were controlled through the dedicated software Dimatix Drop Manager (Fujifilm). We designed three geometries, the full pattern that covers the MEA's active area (Supplementary Figure S1a), the grid pattern that connects the MEA's electrodes (Supplementary Figure S1b) and the network pattern which is composed of micronetworks (Supplementary Fig. S1c). In addition, to demonstrate the alignment efficiency by printing at two different times, the network geometry was disassembled into two parts (Supplementary Fig. S1d and S1e). The printing parameters used were a piezoelectric voltage of 40 V, frequency of 10 kHz, cartridge height of 350µm and printhead temperature of 23 °C. Patterns were printed both on glass coverslips and on micro-electrode arrays (MEAs, 60 electrodes, TiN/SiN, 30 µm electrode diameter, 200 µm spaced, MultiChannel System). Before printing, glass coverslips and MEAs were cleaned by soaking in a 2% v/v solution of Extran MA2 (Merk) for 1 hour, then they were rinsed thoroughly with distilled water and finally dried under N_2 flux. A preliminary analysis of the characteristics of single drops deposited on the substrate was carried out by fluorescence microscopy, disperding FluoSpheres^{TM} Carboxylate-Modified Microspheres (Thermofisher, 0.2 µm diamater, red fluorescent) into the ink and using an Olympus BX-51 upright microscope. To evaluate pattern print fidelity, optical micrographs were captured using an inverted optical microscope (IX-51 Olympus microscope) equipped with a SC180 digital camera and with a C Plan (10 N.A.). The photothermal effect of the CHI-GNRs full pattern on the MEA chip was evaluated in cell culture condition (i.e., with 1 mL of medium). The MEA modified with the full pattern was stimulated under the same conditions as the ink, but the temperature change was measured with a thermocouple (FLUKE).

2.6. Impedance measurement

The electrical properties of MEAs were evaluated by measuring the impedance before and after the patterns deposition. The impedance of the samples was measured adding 1 mL of 1X PBS each, using a potentiostat (Interface 1010E, Gamry Instruments, USA) applying an ac voltage (V_{in} =100 mV_{pp}, f = 1000 Hz).

2.7. Pattern thickness measurements

Pattern thickness was measured using atomic force microscopy (AFM). Sample images were collected using Nanowizard JPK Bioafm (Bruker) operating in QITM mode in water at ambient conditions. MLCT-BIO probe (Bruker), having nominal length 140 µm, tip radius 20 nm, spring constant 0.1 N/m, was used and the images were acquired in height (topography) channels. The raw AFM imaging data obtained were processed and analysed using JPK NanoWizard® SPM and DP software v.6.0 software (Bruker).

2.8. Cell culture

2.8.1. Primary rat neurons

Hippocampal neurons were obtained by dissection from Sprague–Dawley embryonic rats at gestational day 18-19 (E18-E19). After the extraction of embryos, the cerebral tissue was isolated and Hippocampi were exposed to an enzymatic solution of Trypsin 0.125% and DNAse 0.05%, diluted in Ca^{++} and Mg^{++} free Hanks' solution (Gibco Invitrogen), for 18–20 min at 37°C in a water bath. Enzymatic digestion was interrupted by adding culture medium (Neurobasal, Gibco) supplemeted with 10% fetal bovine serum (FBS, Sigma-Aldrich), then the tissue was mechanically triturated with a smoothly fire-tipped Pasteur pipette. The obtained neuronal population was suspended by dilution with plating medium: Neurobasal supplemented with 1% stable L-Glutamine (GlutaMAX 100x, GIBCO Invitrogen), 2% B-27 Supplement (GIBCO Invitrogen), and 1% Pen-Strep (Penicillin–Streptomycin Solution, GIBCO Invitrogen) without serum. No antimitotic drug was used to avoid glial cells proliferation. The experimental protocol was approved by the European Animal Care Legislation (2010/63/EU), by the Italian Ministry of Health following the D.L. 116/1992, and by the guidelines of the University of Genova (Prot. 75F11.N.6JI, 08/08/18). All efforts were made to reduce the number of animals used for the project and to minimize their suffering.

2.8.2. h-iPSCs derived neurons (iNeurons)

To validate the proposed model with human cells, we also performed cultures with neurons obtained from Human-derived induced pluripotent stem cells (h-iPSCs). We used an already characterized reverse tetracycline-controlled transactivator/neurogenin-2 (rtTa/NgN2) positive cell line of h-iPSCs episomial reprogrammed from fibroblast withdrawn from a healthy donor (kindly provided by Donders Institute for Brain, Cognition, and Behavior, Nijmengen, Netherlands) [51]. To stimulate the production of NgN2 neuronal determinant, and induce neuronal differentiation into excitatory cortical neurons, cells were exposed to doxycycline (4 µg/ml in the medium) [49]. For the preparation of the cells, we referred to the protocol described by Frega et al. [51].

For the healthy development of neuronal populations, glial cells play a key role, for this reason iNeurons were mixed and co-culture with cortical astrocytes obtained from dissection of rat embryos E18. Cells were suspended in a complete medium composed by Neurobasal (Thermo Fisher Scientific) supplemented with B-27 supplement (Invitrogen), GlutaMAX (Invitrogen), 10 ng/ml human-BDNF (BioConnect), 10 ng/ml human-NT-3 (BioConnect), 4 µg/ml Doxycycline (Sigma Aldrich) and 1% pen/strep (Sigma Aldrich). To ensure an adequate compromise between neuronal support and astrocytic proliferation, the iNeurons to astrocytes initial ratio was set to 1:1 [51].

2.9. Preparation of 2D neuronal networks on patterns

After the printing process, plating was carried out by using a donuts-shaped Poly-dimethyl-siloxane (PDMS) ring, having a surface area of $\sim$ 28 mm^2 (internal and external diameters: 6 and 16 mm respectively, height: 500 µm) to confine the printed surface.

The day before plating, printed glass coverslips and MEAs were exposure to EtOH 70% for 1 h to ensure complete sterilization. Afterwards, the samples were washed by rinsing with sterile water 3 times to remove EtOH, before being normalized in cell culture medium. To evaluate the cytotoxicity effect of GNRs on neurons, cultures were prepared both on CHI and CHI-GNRs printed patterns. On the plating day, normalization medium was removed from the substrates and neuronal cells were plated directly onto the patterned surface inside the PDMS ring constrain. Specifically,

both neuronal populations were plated at a cell density of 400–600 cell/mm^2.

2.10. Morphological characterization of neuronal networks by immunocytochemistry

Primary neurons (DIV 21) and iNeurons (DIV 42) networks were fixed by exposure for 30 min at room temperature to 4% paraformaldehyde solution in phosphate buffer solution (pH=7.4). Permeabilization was achieved with PBS containing 0.5% TritonX100 for 15 min at room temperature. To avoid non-specific binding of antibodies, samples were exposed for 45 min to blocking buffer solution consisted of PBS, 0.3% BSA (bovine serum albumin Sigma) and 0.5% FBS. We used as primary antibody Microtubule Associated Protein 2 (MAP-2) to label neuronal dendrites (dilution 1:500, monoclonal or polyclonal - Synaptic System), Glial Fibrillary Acidic Protein (GFAP) to label glial specific filament protein (dilution 1:1000, monoclonal or polyclonal antibodies - Sigma) and Dapi to label cells nuclei (dilution, 1:10,000 - Sigma). Samples were incubated with primary antibodies for 1:30 h at room temperature. Afterwards, samples were rinsed with PBS twice before being exposed for 1 h to the secondary antibodies: Alexa Fluor 488, Alexa Fluor 633 Goat anti mouse or Goat anti rabbit, diluted 1:700 and 1:1000 (Invitrogen Life Technologies S. Donato Milanese). Finally, samples were rinsed twice with PBS and stored at 4 °C.

2.11. Neural recording and data analysis

Electrical signals from neural networks were obtained at 21 DIV for the rat and at 28-42 DIV for the iNeurons. The activity from the patterned cell culture was recorded using a standard MEA1060 system (MEA 1060-Inv-Standard amplifier, Multichannel Systems, Germany). The recording conditions were maintained at 37 °C and 5% CO2 by a heating plate and humidified gas, respectively. Collected data were processed using MATLAB (Mathworks) and the Spycode toolset [52]. Digitized signals were filtered with a digital second-order Butterworth high-pass filter (cut-off frequency: 200 Hz) and the spike detection was performed using the threshold based 'Precise Timing Spike Detection' (PTSD) algorithm [53] with a detection threshold set at 8 times the standard deviation of the background noise.

Recording channels whose mean firing rate (MFR) was larger than 0.1 spikes/sec were selected as active channels and used for neural activity analysis. For the photothermal stimulation, a fiber-optic laser (785 nm, 450 mW, B&W Tek) was used for a light source and the laser beam from the bottom formed a 5 mm diameter of illumination area on the MEA chip. The stimulation protocol consists of 20 cycles, where each cycle has 20 s of the laser off followed by 10 s of laser on. For the activity analysis, peri-event time histogram (PSTH) with a 100 ms binsize was used with the NIR irradiation as an event. We define MFR(ON) as the average firing rate when the laser is on, while MFR(OFF) corresponds to the average firing rate calculated in 10 s just before the laser stimulation. The inhibition percentage (IP) of neuronal activity was calculated by the following formula:

$$IP\ [\%] = [1 - MFR(ON) / MFR(OFF)] * 100$$

2.12. Statistical analysis

All result are expressed as mean ± standard deviation (SD) and statistical analysis was performed using Prism (GraphPad Software Inc., CA, USA). Unpaired t-test was used to determine significant differences (statistically significant at $P < 0.05$).

3. Results

3.1. Viscosity and contact angle

To create an ink with suitable printing characteristics, viscosity tests were performed as a first step. Keeping the concentration of acetic acid fixed at 0.1 M, the results obtained for CHI solutions at 1% w/v showed a viscosity equal to 39.2 ± 3.1 cP, a value that drops down to 4.7 ± 0.3 cP for a concentration of 0.1% w/v (Fig. 1a). Contact angle tests on glass smooth surface were made by comparing the values measured at different molarities of acetic acid, both in pure aqueous solutions and in the presence of dissolved CHI. The results showed a linear decrease of the contact angle from 68.6 ± 3.4° for deionized water to 42.5 ± 1.4 ° for 1 M acetic acid solution (Fig. 1b). A similar trend was obtained for the CHI solutions which showed a slight decrease in the contact angle of just about 1.5° with respect to the acetic acid controls.

3.2. CHI-GNRs synthesis and characterization

We synthesized GNRs using a seed-mediated method and characterized them using a UV–visible spectrophotometer and TEM. Fig. 2a shows the UV-spectrum of GNRs presenting the two characteristic peaks that suggest a rod shape, transversal and longitudinal, with the latter tuned close to the laser wavelength source (i.e., 785 nm). The GNRs morphology was evaluated from TEM micrographs, which confirmed the rod shape with an average length of 44.1 ± 4.4 nm, an average width of 11.7 ± 1.4 nm, and an average aspect ratio of 3.9 ± 0.6. After the synthesis, GNRs were dispersed into a 0.5% CHI solution. The CHI-GNRs solution spectrum reported in Fig. 2a shows that the GNRs are colloidally stable inside the CHI solution, uniformly dispersed without any aggregation phenomena. CHI-GNRs dispersion maintained the GNRs optical properties with a slight redshift of the longitudinal peak. Afterwards, we evaluated the rheological properties of CHI-GNRs ink at different nanoparticulate concentration (OD). We found that the viscosity of the dispersion seem not to be affected by the concentration of the nanoparticles for the range considered (0 to 8OD). In fact, In fact, a decrease of the viscosity just from 14 cP for CHI to 13 cP for CHI-GNRs 8OD was found (Fig. 2b). Although a slight increase occurs for the contact angle, from about 41° of the CHI ink to approximately 43° of CHI-GNRs 8 OD (Fig. 2c), this difference is contained in the standard deviation bar. Finally, we evaluated the thermoplasmonic properties of the CHI-GNRs ink measuring the temperature change at different laser power, for 2, 4 and 8 OD cases. Fig. 2d showed that by increasing the laser power the heat released increased too. At a laser power of 450 mW, the temperature reached 24, 34 and 42 °C for 2, 4 and 8 OD, respectively.

3.3. Pattern printing and characterization

To verify the print resolution, we deposited single drops of the ink on a glass substrate (Fig. 3a) and measured their diameter, which is close to 50 µm. Later we printed on MEA 3 different geometries, such as full (Fig. 3b), grid (Fig. 3c), and network patterns (Fig. 3d). About the network pattern, we first print two µ-networks with CHI ink (left side of Fig. 3d) and then we added another µ-network using CHI-GNRs ink (right side of Fig. 3d), showing how it is possible to obtain a perfectly aligned structure also by printing at different times with different inks. Once verified that the print precision does not depend on the pattern geometry, we focused on the full pattern as proof of concept of this work. We acquired the AFM images of the pattern border (Fig. 3e shows an example) and calculated the height difference between the MEA substrate and the pattern, obtaining a pattern thickness measure of 478 ± 29,8 nm (N=6).

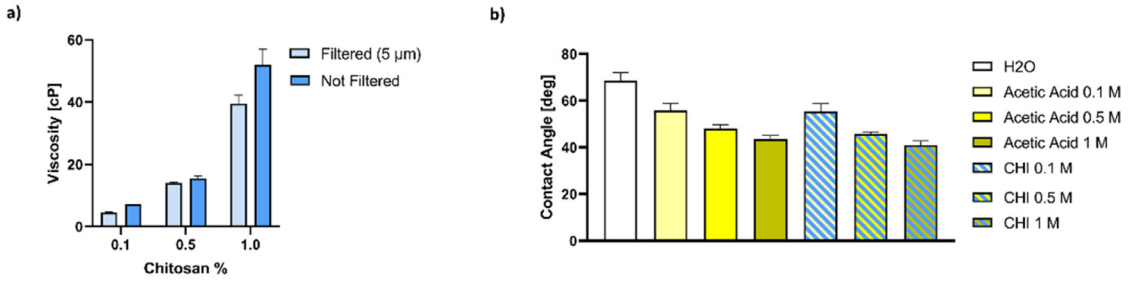

Fig. 1. CHI ink characterization. a) Viscosity of CHI ink (filtered and not) at different chitosan concentrations ($N = 3$, mean ± SD). b) Contact angle measurements of filtered 0.5% CHI ink at different acetic acid molarity compared with the same acetic acid solution molarity and pure water (N=3, mean ± SD).

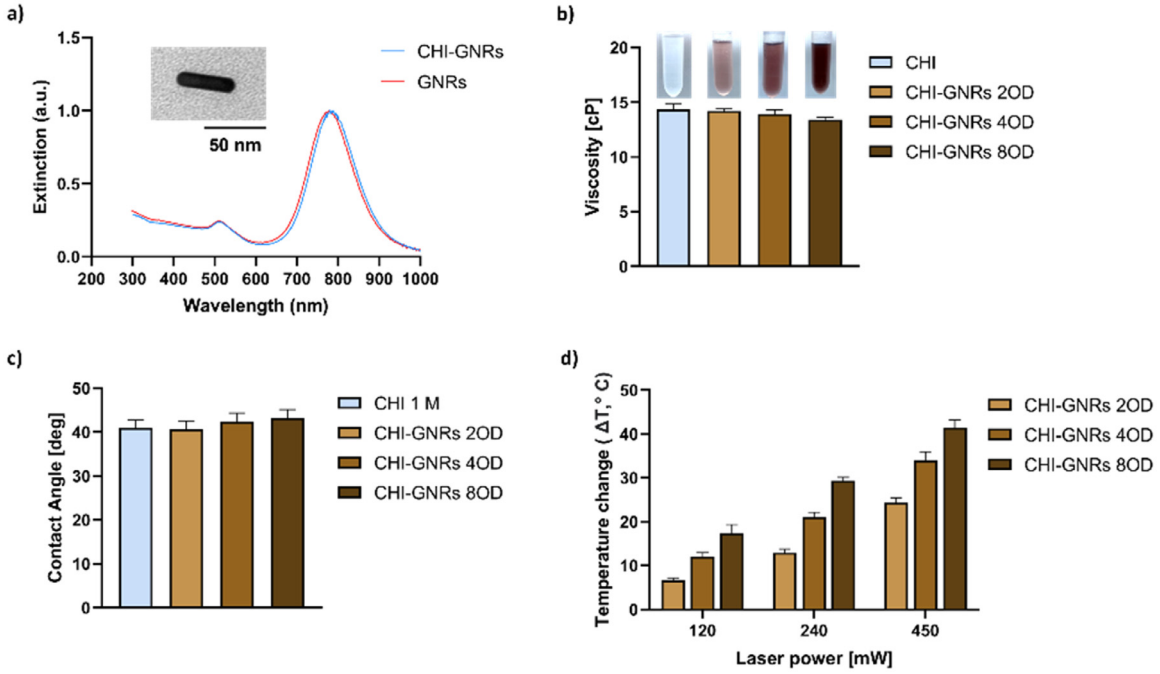

Fig. 2. CHI-GNRs ink characterization. a) Spectrum of GNRs and CHI-GNRs ink with GNR, and TEM image of a single GNR. b) Inks at different OD with their viscosity measurements (N=3, mean ± SD). c) Inks contact angle measurements at different OD (N=3, mean ± SD). d) CHI-GNRs ink temperature change measurement in air at different OD and laser power (N=3, mean ± SD).

To verify that the pattern thickness does not change the MEA electrical properties significantly, we measured the impedance module (Fig. 3f) and phase (Fig. 3g) of the bare MEA, MEA with CHI pattern and MEA with CHI-GNRs pattern. The impedance module increases from approximately 130 kΩ without any pattern to approximately 250 kΩ with a CHI pattern and finally drop to approximately 225 kΩ with CHI-GNRs pattern, while the impedance phase remains stable around -56°.

Finally, we investigated how the temperature changed in cell culture conditions if the patterned MEA was stimulated with different laser power. Fig. 3h shows that increasing the laser power is possible to control also the amount of heat released up to a temperature rise of approximately 9 °C at 450 mW. In contrast, at the same laser power, the medium temperature change of the control samples is significantly lower (Fig. 3i).

3.4. Morphological and electrophysiological characterization of primary neuronal networks

Phase contrast and fluorescence optical microscopies were carried out to evaluate the bioaffinity of CHI-GNRs patterns to primary neurons. From the images shown in Fig. 4a, it can be observed how, after 21 days *in vitro* (DIV21), the cells adhere only to the printed patterns, as demonstrated by the presence of neurites and healthy neurons. Immunofluorescence characterization was carried out to analyze the structure and composition of the planar patterned networks. Samples were labeled using MAP-2 (green), GFAP (red) and DAPI (blu). As can be observed in Fig. 4b, a dense network with a homogenous distribution of neuronal and glial cell populations was developed. Furthermore, Fig. 4c shows how neurons were able to follow more complex patterns and geometries, such as grid patterns.

To verify the ability of the pattern to sustain adhesion and neuronal activity recording, we used primary hippocampal neuronal rat cells that they are usually considered the gold standard in electrophysiological *in vitro* studies. At 21 DIV the patterned cell cultures, which have an average MFR of 2.448 ± 0.07 spks/sec ($N = 3$), were stimulated with NIR light following the protocol described in Section 2.11. Fig. 4d shows the PSTH of an MEA electrode, where the inhibitory phenomenon is ideally within 10 s of stimulation, and its magnitude increases as the laser power increase. The raw data of one electrode is shown in Fig. 4e, where it can be seen that neuronal activity is modulated only during the stimulation cycle and resumes normally once this is over. Fig. 4f shows an average electrodes inhibition percentage of a MEA chip with a CHI-GNRs patterned hippocampal culture, where the inhibition per-

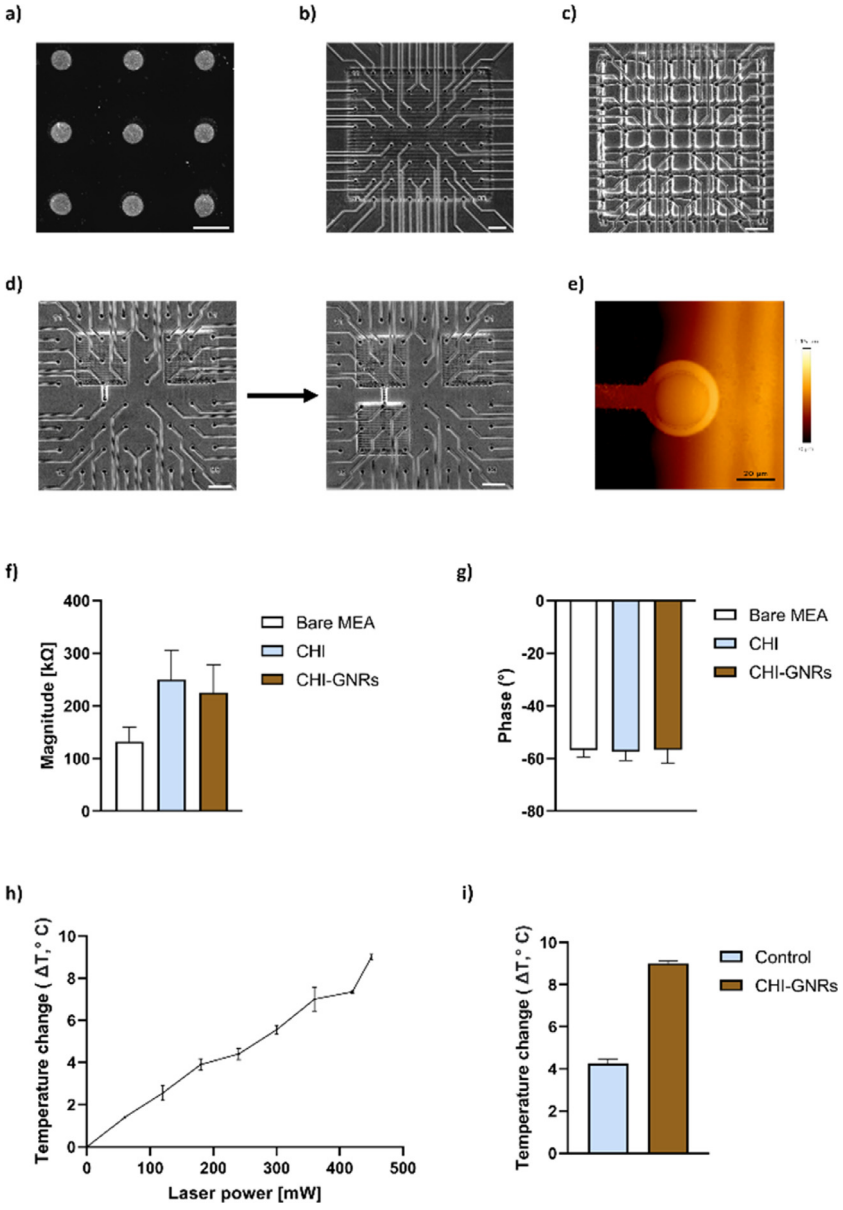

Fig. 3. Patterns printing and characterization. a) Fluorescence image of CHI-GNRs single drops labeled with FluoSpheres; scalebar = 100 µm. b) Contrast phase image of a CHI-GNRs full pattern on MEA; scalebar = 200 µm. c) Contrast phase image of a CHI-GNRs grid pattern on MEA (scalebar = 200 µm). d) Contrast phase image of network pattern on MEA developed in two steps: CHI network pattern (left) CHI network pattern with an additional CHI-GNRs network (right); scalebar = 200 µm. e) AFM image of a CHI-GNRs full pattern border section. f) Impedance module measured for bare MEA (N = 57), MEA with CHI pattern (N=57) and for MEA with CHI-GNRs pattern (N=54). Mean ± SD. g) Impedance phase measured for bare MEA (N = 58), for MEA with CHI pattern (N=57) and for MEA with CHI-GNRs pattern (N=57). Mean ± SD. h) Temperature change measurement in cell culture condition for CHI-GNRs full pattern on MEA at different laser power (N=2). Mean ± SD. i) Temperature change measurement in cell culture condition for MEA with and without (control) CHI-GNRs full pattern at 450 mW. Mean ± SD.

centage means the decrease of the electrode MFR. As the laser power increased, the percentage of inhibition also increased, from 40% stimulating with 120 mW up to about 60% with 450 mW. Finally, Fig. 4g shows that with the same laser power, the inhibition percentage is significantly higher in CHI-GNRs compared to the control.

3.5. Morphological and electrophysiological characterization of human neuronal networks

After testing the pattern efficiency with primary neurons, we validated the model with iNeurons. iNeurons show similar results to those observed for primary neurons. Cells faithfully followed the printed pattern (Fig. 5a), adapting also to fine geometries (Fig. 5b and 5c) and formed a dense network on the patterns. Moreover, from immunofluorescence characterization, it was possible to highlight a peculiar and defined organization of the two cell populations on the 2D square pattern, with neuronal cells creating a concentric square inside the glial one (Fig. 5d). In particular, by a 50x objective it was possible to observe that neurons had an *in vivo*-like shape, showing a round soma from which neuritic arborizations originate, while GFAP-positive cells presented thin morphology [54]. iNeurons patterned cultures were stimulated starting from 28 DIV with the same protocol and conditions used for the primary ones. Fig. 5e shows the average electrodes inhibition percentage of a MEA chip with iNeurons onto a CHI-GNRs pattern, at different DIV and under different laser power. Also in this case the inhibition percentage can be controlled by changing the laser

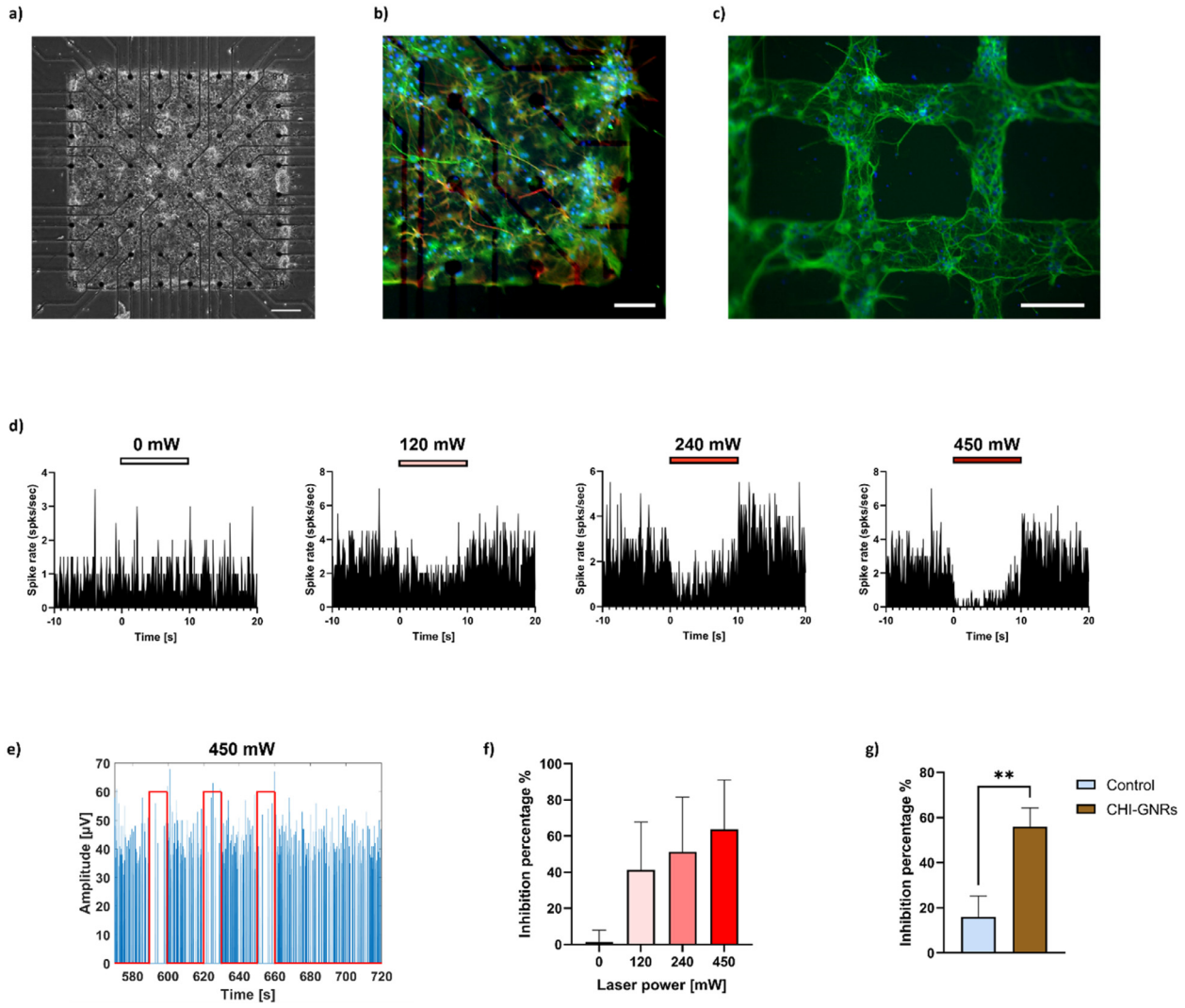

Fig. 4. Morphological and electrophysiological characterization of primary rat pattern neuronal network. a) Contrast phase image of a CHI-GNRs full patterned neuronal network (DIV 21); scalebar = 200 µm. b) Immunochemistry staining images of a CHI-GNRs full patterned neuronal network (DIV 21) corner labeled with MAP-2 (green), GFAP (red) and DAPI (blue); scalebar = 100 µm. c) Immunochemistry staining images of a CHI-GNRs grid patterned neuronal network labeled with MAP-2 (green) and DAPI (blue); scalebar = 100 µm. d) PSTH of a MEA electrode with CHI-GNRs patterned neuronal network at different laser power. e) 150 s of spike train with analog data at 450 mW. f) Inhibition percentage with CHI-GNRs patterned neuronal network at different laser power (mean ± SD, electrodes number = 34, 36, 36, 34). g) Inhibition percentage at 450 mW (mean ± SD, $N = 3$ both for control and CHI-GNRs, Unpaired t-test, p-value = 0.0053). (For interpretation of the references to color in this figure legend, the reader is referred to the web version of this article.)

power, reaching an approximately value of 60%, 70% and 80% at 28, 35 and 42 DIV respectively using a laser power of 450 mW. Focusing on the middle timepoint (i.e., 35 DIV), Fig. 5f shows an example electrode PSTH where it is possible to observe how, like the primary neurons patterned culture, the inhibition percentage was well confined inside the 10 s NIR light stimulation, while Fig. 5g shows as the laser stimulation affected the spike train at 450 mW. Fig. 5h shows the significant gap between control and CHI-GNRs samples at 450 mW. Indeed, if the control reached an average inhibition percentage of 30%, with the same laser power CHI-GNRs pattern reached almost 80%. Finally, Fig. 5i reports changes in the MFR as the number of DIV increases.

4. Discussion

As a first step the CHI-GNR ink properties were characterized in terms of viscosity and of thermoplasmonic effect. As relates to the viscosity, the printer used in this work requires an ink with a viscosity close to the range of 10-12 cP as a reference parameter [55]. In this respect, the 0.5% w/v CHI solution, having a viscosity of 14.36 ± 0.48 cP, was selected as ink. This value is slightly higher than the limit recommended by the manufacturer of the instrument, however the tests we carried out by dispersing the GNRs in solution have shown how the addition of the particles until a concentration of 8 OD does not lead to a significant change in the viscosity. By dispersing GNRs in this solution, the viscosity decreased to a value of 14.20 ± 0.25, 13.94 ± 0.37 and 13.39 ± 0.23 cP respectively for CHI-GNRs 2, 4 and 8 OD (Fig. 2b), obtaining a viscosity closer to the optimal print values. A probable light decrease of the viscosity that can be observed by adding the GNRs might be associated with the dilution due to the addition of deionized water used as dispersant of the particles that are added directly to the CHI solution. A different concentration of acetic acid does not affect the viscosity of the dissolved chitosan solutions as already demonstrated by Geng et al. [56]. However, as previously reported in the literature, acetic acid, in addition to favoring the dissolution of CHI in aqueous solutions, lowers the surface tension of the water solution as its concentration increases [57], acting as a non-

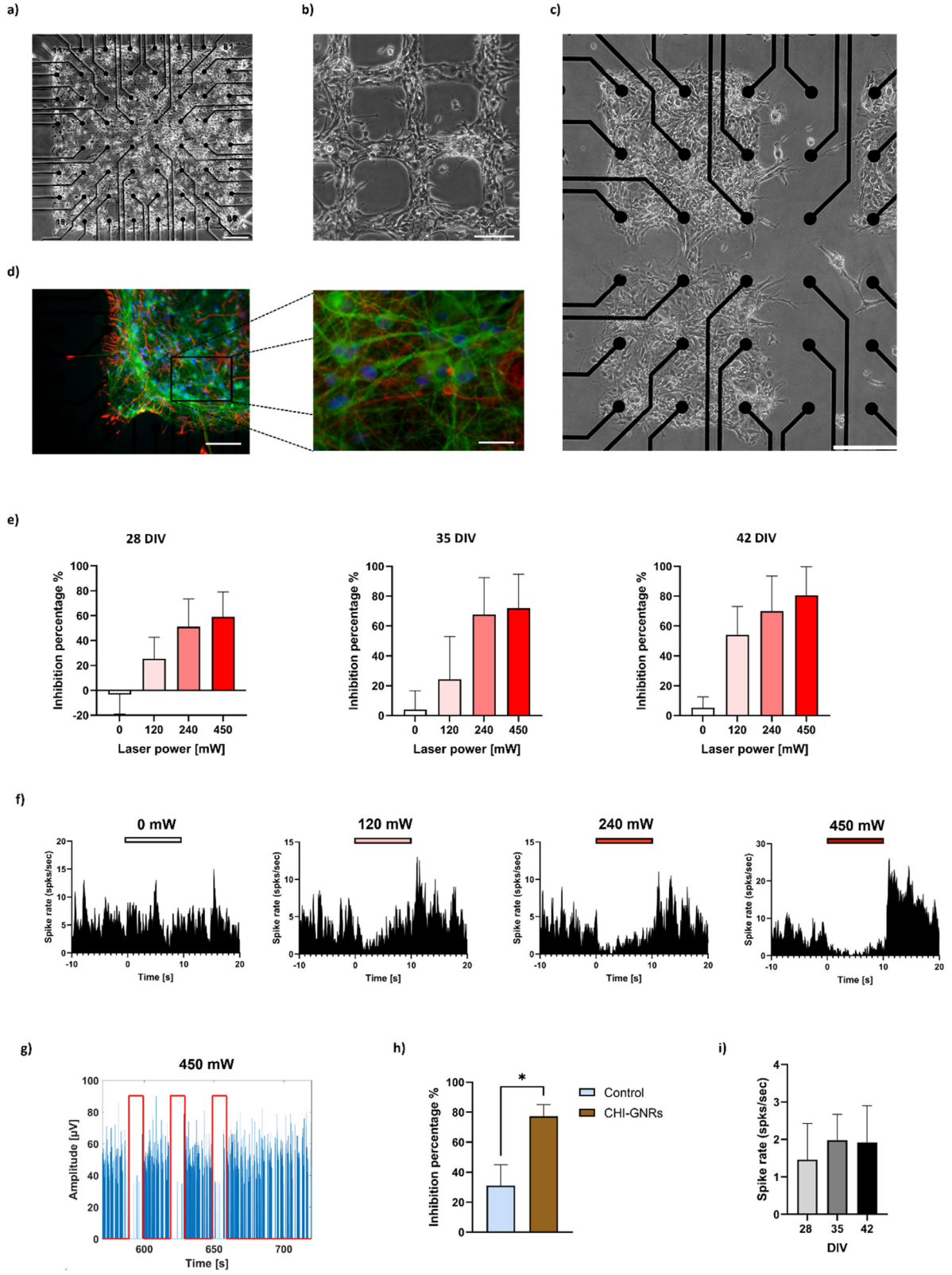

Fig. 5. Morphological and electrophysiological characterization of iNeurons pattern neuronal network. a) Contrast phase image of CHI-GNRs full patterned neuronal network; scalebar = 200 μm. b) Contrast phase image of CHI-GNRs grid patterned neuronal network (DIV 15); scalebar = 100 μm. c) Contrast phase image of patterned neuronal network: upper μ-network was made with CHI ink, lower μ-network was made with CHI-GNRs ink; scalebar = 200 μm. d) Immunochemistry staining images of a CHI-GNRs full patterned neuronal network (DIV 42) corner labeled with MAP-2 (green), GFAP (red) and DAPI (blue); left scalebar = 100 μm, right scalebar = 20 μm. e) Inhibition percentage for CHI-GNRs patterned neuronal network at different laser power and measured at DIV 28 (elecrodes number = 18, 17, 17, 19), DIV 35 (electrodes number = 24, 25, 23, 25) and DIV 42 (electrodes number = 13, 13, 12, 10). Mean ± SD. f) PSTH CHI-GNRs patterned neuronal network at different laser power (DIV 35). g) 150 s of spike train with analog data at 450 mW. H) Inhibition percentage at DIV 35 with a laser power of 450 mW (mean ± SD, $N = 3$ for control and $N = 5$ for CHI-GNRs, Unpaired t-test, p-value < 0.05). i) CHI-GNRs patterned neuronal network MFR at different DIV (mean ± SD, $N = 5$ for each DIV). (For interpretation of the references to color in this figure legend, the reader is referred to the web version of this article.)

ionic surfactant. A systematic study, made by Alvarez et al. on the surface tension of solutions of acetic acid diluted in water, demonstrate that, at increasing concentrations of acetic acid, there was a decrease in the surface tension [58]. We have evaluated the effect of the acetic acid concentration on the surface tension of our formulations in an indirect way by analyzing the contact angle between the liquid phase and a smooth glass surface. The contact angle values were found to decrease with the molarities increasing, showing the same linear trend under equal conditions as demonstrated by Alvarez et al. for surface tension. The results obtained for the contact angle of the chitosan-based solutions, under the same measurement conditions, showed values comparable to those obtained for the aqueous solutions of pure acetic acid. Indeed, it is reasonable to speculate that even in terms of interfacial interaction between liquid and glass solid surface, the addition of chitosan in solution, also considering the low final concentration of the polymer, does not lead to any variation. In fact, in our study acetic acid has the double function of solvent and surfactant, making its concentration in solution the only parameter to be adjusted for printing.

The ink temperature tests in air condition showed that the CHI-GNRs 4 OD ink, at 450 mW, increased the temperature of at least 30 C°, which is considered sufficient to obtain a good level of inhibition of the neuronal network activity [36]. This ink was used for the subsequent experiments. The GNRs surface density on MEA for 4OD was around $1.5 * 10^7$ GNRs/mm^2.

As shown in Fig. 3a, the print resolution obtained was found to be comparable to the MEA electrode (i.e., 30 μm). All the geometries were printed with good precision, demonstrating the great versatility and simplicity of the used technique. In addition to full geometry (Fig. 3b), simple condition chosen to demonstrate the control of the activity by thermoplasmonic effect, it was possible to realize more complex structures such as the grid (Fig. 3c), connecting only the MEA electrodes, or as micro-networks (Fig. 3d). For example, this geometry could be used to realize neuronal microenvironments linked together and analyze how the activity affects the other. As the figure shows, thanks to the easy alignment allowed by the software, with this technique, it was possible to realize portions of patterns at different times, managing to reconstruct the overall geometry precisely.

Although the thickness of the pattern was found to be ∼500 nm, the impedance test excluded any possible interference in the subsequent neuronal activity recording. Impedance analysis showed that the pattern did not affect the impedance phase and even if the impedance module values were increased, it remained around the hundreds of kΩ (Fig. 3e), not precluding the recording of neuronal activity [36]. Furthermore, the presence of GNRs leaded to a slight improvement in the device's electrical properties compared to the pattern without GNRs, in agreement with the results found by Yoo et al. [36]. Finally, the temperature test in cell culture condition confirmed that the CHI-GNRs patterned MEA reached a temperature change sufficient to modulate the neural activity by thermoplasmonic effect [35]. Based on the data found in the literature on the cumulative temperature rise at the medium interface, it is reasonable to assume that the temperature rise at the cell interface at the stimulation time is about 5 °C or less [59,60]. This value is reasonable, considering that the increase in temperature did not damage the cells. Although the control samples leaded to a slight increase in temperature too, this was significantly lower.

As a second step, the cytotoxity and bioactivity of the CHI-GNRs ink were evaluated. In this respect the adhesion of the cells was verified. This characterization was performed on full pattern (Figs. 4a and 5a), grid patterned with 50 μm thick lines (Figs. 4c and 5b) and on micro-networks connected each other's (Fig. 5c). The results obtained showed that both neurons and glial cells adhered to the print patterns, confirming the bioactivity of chitosan [23,24], which was not compromised by the addition of the GNRs [61]. The stability of the neuronal networks over time (up to DIV 42) was also assessed, making CHI an interesting candidate for long term cultures.

The effectiveness of this approach was demonstrated for both primary rat cells and human iNeurons. This represents a valuable contribution in the search for low-cost biomimetic culture systems, which can have important applications in neuropharmacology, toxicology, and regenerative medicine.

As a first step the thermoplasmonic properties of the developed pattern was verified using primary rat neurons in order to compare the obtained results with the literature on this topic. We demonstrated that by increasing the laser power it was possible to increase the inhibition activity of patternated neuronal networks. Although an inhibitory phenomenon is present even without GNRs, this is significantly lower than in samples with nanoparticles (i.e., CHI-GNRs). We speculate that the mild inhibitory phenomenon without GNRs is probably due to the MEA's metal component heating when irradiated by NIR light. The results obtained in this work are consistent with those obtained using the same cells and the same laser with very similar powers by Yoo et al. [36], confirming the good thermoplasmonic properties of our patterns. However, there is a slight difference in the inhibition percentage, considering we reach about 25% less of those reported in [36] with similar laser power. The lower level of inhibition may be due to the different interface conditions between cells and GNRs. In fact, in Yoo et al., the cells are sown in direct contact with a layer of GNRs, while in our case, the GNRs are inside a biopolymeric layer having a thickness of about 500 nm. Finally, although an inhibitory phenomenon is present even without GNRs, this is significantly lower than in samples with nanoparticles (i.e., CHI-GNRs). We speculate that the mild inhibitory phenomenon without GNRs is probably due to the heating of the device components under NIR irradiation, where the metal part (i.e., electrodes) plays the major role. Indeed, in our recent paper, we found that limiting the electrodes contributes the gap between the control group and the test group increase significantly [62].

The thermoplasmonic properties of the CHI-GNRs pattern were then also characterized using human iNeurons. As far as we know, this is the first work where the thermoplasmonic effect was used to inhibit the electrophysiological activity of human iNeurons. From Fig. 5e and 5i it is possible to conclude that the pattern is stable. Indeed, the pattern preserves both its thermoplasmonic properties, which allow to obtain a consistent level of inhibition as DIV increases (Fig. 5e) and its bioadhesive properties, which allows a consolidation of the network that develops-stabilizes and remains electrically active (Fig. 5i). Furthermore, for both human and rat neuronal networks, the inhibition of the activity by photothermal effect is fully reversible (Figs. 4e and 5g) and confined within the stimulation period (Figs. 4d and 5f), demonstrating a high temporal control also on the modulation effect. Finally, although it is not the aim of this study, from a preliminary comparison between the two cell types, we can speculate that under the same condition human neurons (Fig. 5h) appear to be more sensitive to the photothermal stimulation than rat ones (Fig. 4g).

Although not the subject of study in this paper, the realized photosensitive micropatterned platform opens the door to new methods for studying the connectivity *in vitro* of a neuronal network. With the controlled deposition of adhesion factor and gold nanorods, different geometries with photosensitive and no photosensitive areas can be easily, quickly, and economically fabricated. This provides a complete platform in which it is possible to record the activity of a patterned neuronal network, excite it locally by electrical stimulation (using MEA microelectrodes [31]), and inhibit it locally by photothermal stimulation. Among possible future de-

velopments, we consider fascinating the neuronal activity study of unstimulated regions directly connected to the areas under photothermal and electrical stimulation.

5. Conclusions

In this work, a bioactive and photosensitive ink was designed, developed and printed by ink-jet technology using a commercial piezoelectric printer. The printed photosensitive patterns were used to control the structure and activity of neural networks, without the use of any physical master and without the need of further functionalization with adhesion factors. Both rat and human-derived neural networks were tested with the developed photosensitive patterns. To our knowledge this is the first evidence of photothermal stimulation inhibiting human neuronal activity. The approach proposed in this work provides a useful tool for the study of neuronal communication and associated disorders, in a high reproducible and low cost manner.

Declaration of Competing Interest

The authors declare no competing financial interest.

CRediT authorship contribution statement

Andrea Andolfi: Investigation, Methodology, Validation, Data curation, Writing – original draft. **Pietro Arnaldi:** Investigation, Validation, Data curation, Writing – original draft. **Donatella Di Lisa:** Supervision, Methodology, Data curation. **Sergio Martinoia:** Supervision, Writing – review & editing. **Laura Pastorino:** Conceptualization, Supervision, Writing – review & editing.

Acknowledgments

Katia Cortese and Maria Cristina Gagliani for electronic micrographs acquisition. Marina Delucchi for providing us with the necessary impedance characterization tool.

Supplementary materials

Supplementary material associated with this article can be found, in the online version, at doi:10.1016/j.actbio.2022.12.036.

References

[1] S. Bang, S. Jeong, N. Choi, H.N. Kim, Brain-on-a-chip: a history of development and future perspective, Biomicrofluidics 13 (2019) 051301, doi:10.1063/1.5120555.
[2] T. Cameron, T. Bennet, E. Rowe, M. Anwer, C. Wellington, K. Cheung, Review of design considerations for brain-on-a-chip models, Micromachines (Basel) 12 (2021) 441, doi:10.3390/mi12040441.
[3] B.C. Wheeler, G.J. Brewer, Designing neural networks in culture, Proc. IEEE 98 (2010) 398–406, doi:10.1109/JPROC.2009.2039029.
[4] B. Mossink, A.H.A. Verboven, E.J.H. van Hugte, T.M. Klein Gunnewiek, G. Parodi, K. Linda, C. Schoenmaker, T. Kleefstra, T. Kozicz, H. van Bokhoven, D. Schubert, N. Nadif Kasri, M. Frega, Human neuronal networks on micro-electrode arrays are a highly robust tool to study disease-specific genotype-phenotype correlations in vitro, Stem Cell Rep. 16 (2021) 2182–2196, doi:10.1016/j.stemcr.2021.07.001.
[5] A. Pelkonen, C. Pistono, P. Klecki, M. Gómez-Budia, A. Dougalis, H. Konttinen, I. Stanová, I. Fagerlund, V. Leinonen, P. Korhonen, T. Malm, Functional characterization of human pluripotent stem cell-derived models of the brain with microelectrode arrays, Cells 11 (2021) 106, doi:10.3390/cells11010106.
[6] G. Bruno, N. Colistra, G. Melle, A. Cerea, A. Hubarevich, L. Deleye, F. de Angelis, M. Dipalo, Microfluidic multielectrode arrays for spatially localized drug delivery and electrical recordings of primary neuronal cultures, Front. Bioeng. Biotechnol. 8 (2020), doi:10.3389/fbioe.2020.00626.
[7] T.J. Shafer, Application of microelectrode array approaches to neurotoxicity testing and screening, in: 2019: pp. 275–297. https://doi.org/10.1007/978-3-030-11135-9_12.
[8] E. Tibau, Ch. Bendiksen, S. Teller, N. Amigó, J. Soriano, Interplay activity-connectivity: dynamics in patterned neuronal cultures, in: 2013: pp. 54–63. https://doi.org/10.1063/1.4776501.
[9] N. Hong, Y. Nam, Thermoplasmonic neural chip platform for in situ manipulation of neuronal connections in vitro, Nat. Commun. 11 (2020), doi:10.1038/s41467-020-20060-z.
[10] H. Dermutz, G. Thompson-Steckel, C. Forró, V. de Lange, L. Dorwling-Carter, J. Vörös, L. Demkó, Paper-based patterned 3D neural cultures as a tool to study network activity on multielectrode arrays, RSC Adv. 7 (2017) 39359–39371, doi:10.1039/C7RA00971B.
[11] J.M. Corey, B.C. Wheeler, G.J. Brewer, Compliance of hippocampal neurons to patterned substrate networks, J. Neurosci. Res 30 (1991) 300–307, doi:10.1002/jnr.490300204.
[12] Y. Tanaka, H. Watanabe, K. Shimoda, K. Sakamoto, Y. Hondo, M. Sentoku, R. Sekine, T. Kikuchi, K. Yasuda, Stepwise neuronal network pattern formation in agarose gel during cultivation using non-destructive microneedle photothermal microfabrication, Sci. Rep. 11 (2021) 14656, doi:10.1038/s41598-021-93988-x.
[13] M. Bani-Yaghoub, R. Tremblay, R. Voicu, G. Mealing, R. Monette, C. Py, K. Faid, M. Sikorska, Neurogenesis and neuronal communication on micropatterned neurochips, Biotechnol. Bioeng. 92 (2005) 336–345, doi:10.1002/bit.20618.
[14] C. Wyart, C. Ybert, L. Bourdieu, C. Herr, C. Prinz, D. Chatenay, Constrained synaptic connectivity in functional mammalian neuronal networks grown on patterned surfaces, J. Neurosci. Methods 117 (2002) 123–131, doi:10.1016/S0165-0270(02)00077-8.
[15] A. Rajnicek, S. Britland, C. McCaig, Contact guidance of CNS neurites on grooved quartz: influence of groove dimensions, neuronal age and cell type, J. Cell Sci. 110 (1997) 2905–2913, doi:10.1242/jcs.110.23.2905.
[16] I. Suzuki, Y. Sugio, Y. Jimbo, K. Yasuda, Stepwise pattern modification of neuronal network in photo-thermally-etched agarose architecture on multi-electrode array chip for individual-cell-based electrophysiological measurement, Lab Chip 5 (2005) 241, doi:10.1039/b406885h.
[17] G. Kang, J.-H. Lee, C.-S. Lee, Y. Nam, Agarose microwell based neuronal microcircuit arrays on microelectrode arrays for high throughput drug testing, Lab Chip 9 (2009) 3236, doi:10.1039/b910738j.
[18] E. Macis, M. Tedesco, P. Massobrio, R. Raiteri, S. Martinoia, An automated microdrop delivery system for neuronal network patterning on microelectrode arrays, J. Neurosci. Methods 161 (2007) 88–95, doi:10.1016/j.jneumeth.2006.10.015.
[19] I. Poudel, J.S. Lee, L. Tan, J.Y. Lim, Micropatterning–retinoic acid co-control of neuronal cell morphology and neurite outgrowth, Acta Biomater. 9 (2013) 4592–4598, doi:10.1016/j.actbio.2012.08.039.
[20] B.-J. de Gans, P.C. Duineveld, U.S. Schubert, Inkjet printing of polymers: state of the art and future developments, Adv. Mater. 16 (2004) 203–213, doi:10.1002/adma.200300385.
[21] K.B. Lee, L. Kelbauskas, A. Brunner, D.R. Meldrum, A versatile method for dynamically controlled patterning of small populations of epithelial cells on substrates via non-contact piezoelectric inkjet printing, PLoS One 12 (2017) e0176079, doi:10.1371/journal.pone.0176079.
[22] E. Antonopoulou, O.G. Harlen, M. Rump, T. Segers, M.A. Walkley, Effect of surfactants on jet break-up in drop-on-demand inkjet printing, Phys. Fluids 33 (2021) 072112, doi:10.1063/5.0056803.
[23] D. Di Lisa, M. Tedesco, E. Dellacasa, M. Pesce, T. Catelani, P. Massobrio, R. Raiteri, S. Martinoia, L. Pastorino, Chitosan biopolymer: alternative adhesion factor and scaffold matrix for 2D and 3D neuronal cultures, Biomed. Sci. Eng. 3 (2020) 9–10, doi:10.4081/bse.2019.107.
[24] M.T. Tedesco, D. Di Lisa, P. Massobrio, N. Colistra, M. Pesce, T. Catelani, E. Dellacasa, R. Raiteri, S. Martinoia, L. Pastorino, Soft chitosan microbeads scaffold for 3D functional neuronal networks, Biomaterials 156 (2018) 159–171, doi:10.1016/j.biomaterials.2017.11.043.
[25] P. Arnaldi, D. Di Lisa, L. Maddalena, F. Carosio, A. Fina, L. Pastorino, O. Monticelli, A facile approach for the development of high mechanical strength 3D neuronal network scaffold based on chitosan and graphite nanoplatelets, Carbohydr. Polym. 271 (2021) 118420, doi:10.1016/j.carbpol.2021.118420.
[26] D. Di Lisa, L. Muzzi, S. Pepe, E. Dellacasa, M. Frega, A. Fassio, A. Lagazzo, S. Martinoia, L. Pastorino, On the way back from 3D to 2D: chitosan promotes adhesion and development of neuronal networks onto culture supports, Carbohydr. Polym. 297 (2022) 120049.
[27] A. Andolfi, P. Arnaldi, D. Di Lisa, S. Martinoia, L. Pastorino, Ink-jet printed chitosan precise patterning for engineered 2D neuronal networks, Biomed. Sci. Eng. 4 (2021) 24–25, doi:10.4081/bse.2021.148.
[28] A.T. Sack, Transcranial magnetic stimulation, causal structure–function mapping and networks of functional relevance, Curr. Opin. Neurobiol. 16 (2006) 593–599, doi:10.1016/j.conb.2006.06.016.
[29] T. Sankar, M.M. Chakravarty, A. Bescos, M. Lara, T. Obuchi, A.W. Laxton, M.P. McAndrews, D.F. Tang-Wai, C.I. Workman, G.S. Smith, A.M. Lozano, Deep brain stimulation influences brain structure in Alzheimer's disease, Brain Stimul. 8 (2015) 645–654, doi:10.1016/j.brs.2014.11.020.
[30] S.F. Muldoon, F. Pasqualetti, S. Gu, M. Cieslak, S.T. Grafton, J.M. Vettel, D.S. Bassett, Stimulation-based control of dynamic brain networks, PLoS Comput. Biol. 12 (2016) e1005076, doi:10.1371/journal.pcbi.1005076.
[31] S. Joucla, B. Yvert, Modeling extracellular electrical neural stimulation: from basic understanding to MEA-based applications, J. Physiol.-Paris 106 (2012) 146–158, doi:10.1016/j.jphysparis.2011.10.003.
[32] P.S.A. Kalanithi, J.M. Henderson, Optogenetic Neuromodulation, in: 2012: pp. 185–205. https://doi.org/10.1016/B978-0-12-404706-8.00010-3.
[33] F. Zhang, L.P. Wang, M. Brauner, J.F. Liewald, K. Kay, N. Watzke, P.G. Wood, E. Bamberg, G. Nagel, A. Gottschalk, K. Deisseroth, Multimodal fast optical interrogation of neural circuitry, Nature (2007), doi:10.1038/nature05744.

[34] J.C. Williams, T. Denison, From optogenetic technologies to neuromodulation therapies, Sci. Transl. Med. 5 (2013), doi:10.1126/scitranslmed.3003100.
[35] S. Yoo, S. Hong, Y. Choi, J.-H. Park, Y. Nam, Photothermal inhibition of neural activity with near-infrared-sensitive nanotransducers, ACS Nano 8 (2014), doi:10.1021/nn5020775.
[36] S. Yoo, R. Kim, J.-H. Park, Y. Nam, Electro-optical neural platform integrated with nanoplasmonic inhibition interface, ACS Nano 10 (2016) 4274–4281, doi:10.1021/acsnano.5b07747.
[37] H. Jung, H. Kang, Y. Nam, Digital micromirror based near-infrared illumination system for plasmonic photothermal neuromodulation, Biomed. Opt. Express 8 (2017) 2866, doi:10.1364/boe.8.002866.
[38] R.J. Jakel, B.L. Schneider, C.N. Svendsen, Using human neural stem cells to model neurological disease, Nat. Rev. Genet. 5 (2004) 136–144, doi:10.1038/nrg1268.
[39] L. Kandratavicius, P.A. Balista, C. Lopes-Aguiar, R.N. Ruggiero, E.H. Umeoka, N. Garcia-Cairasco, L.S. Bueno-Junior, J.P. Leite, Animal models of epilepsy: use and limitations, Neuropsychiatr. Dis. Treat. 10 (2014) 1693–1705, doi:10.2147/NDT.S50371.
[40] J.A. Potashkin, S.R. Blume, N.K. Runkle, Limitations of animal models of Parkinson's disease, Parkinsons Dis. 2011 (2011) 1–7, doi:10.4061/2011/658083.
[41] J. Kwon, J.S. Lee, J. Lee, J. Na, J. Sung, H.-J. Lee, H. Kwak, E. Cheong, S.-W. Cho, H.-J. Choi, Vertical nanowire electrode array for enhanced neurogenesis of human neural stem cells via intracellular electrical stimulation, Nano Lett. 21 (2021) 6343–6351, doi:10.1021/acs.nanolett.0c04635.
[42] E. Tomaskovic-Crook, P. Zhang, A. Ahtiainen, H. Kaisvuo, C. Lee, S. Beirne, Z. Aqrawe, D. Svirskis, J. Hyttinen, G.G. Wallace, J. Travas-Sejdic, J.M. Crook, Human neural tissues from neural stem cells using conductive biogel and printed polymer microelectrode arrays for 3D electrical stimulation, Adv. Healthc. Mater. 8 (2019) 1900425, doi:10.1002/adhm.201900425.
[43] Y.-S. Lee, T.L. Arinzeh, The influence of piezoelectric scaffolds on neural differentiation of human neural stem/progenitor cells, Tissue Eng. Part A 18 (2012) 2063–2072, doi:10.1089/ten.tea.2011.0540.
[44] P.S. Balasubramanian, A. Singh, C. Xu, A. Lal, GHz ultrasonic chip-scale device induces ion channel stimulation in human neural cells, Sci. Rep. 10 (2020) 3075, doi:10.1038/s41598-020-58133-0.
[45] F. Schmieder, S. Klapper, N. Koukourakis, V. Busskamp, J. Czarske, Optogenetic stimulation of human neural networks using fast ferroelectric spatial light modulator—based holographic illumination, Appl. Sci. 8 (2018) 1180, doi:10.3390/app8071180.
[46] O. Akhavan, E. Ghaderi, S.A. Shirazian, Near infrared laser stimulation of human neural stem cells into neurons on graphene nanomesh semiconductors, Colloids Surf. B Biointerfaces 126 (2015) 313–321, doi:10.1016/j.colsurfb.2014.12.027.
[47] R. Duan, Z. Zhou, G. Su, L. Liu, M. Guan, B. Du, Q. Zhang, Chitosan-coated gold nanorods for cancer therapy combining chemical and photothermal effects, Macromol. Biosci. 14 (2014) 1160–1169, doi:10.1002/mabi.201300563.
[48] C.-H. Wang, C.-W. Chang, C.-A. Peng, Gold nanorod stabilized by thiolated chitosan as photothermal absorber for cancer cell treatment, J. Nanopart. Res. 13 (2011) 2749–2758, doi:10.1007/s11051-010-0162-5.
[49] P. Matteini, F. Ratto, F. Rossi, S. Centi, L. Dei, R. Pini, Chitosan films doped with gold nanorods as laser-activatable hybrid bioadhesives, Adv. Mater. 22 (2010) 4313–4316, doi:10.1002/adma.201002228.
[50] M. Türk, U. Tamer, E. Alver, H. Çiftçi, A.Ü. Metin, S. Karahan, Fabrication and characterization of gold-nanoparticles/chitosan film: a scaffold for L929-fibroblasts, Artif. Cells Nanomed. Biotechnol. 41 (2013) 395–401, doi:10.3109/21691401.2012.761228.
[51] M. Frega, S.H.C. van Gestel, K. Linda, J. van der Raadt, J. Keller, J.-R. van Rhijn, D. Schubert, C.A. Albers, N.Nadif Kasri, Rapid neuronal differentiation of induced pluripotent stem cells for measuring network activity on micro-electrode arrays, J. Vis. Exp. (2017), doi:10.3791/54900.
[52] L.L. Bologna, V. Pasquale, M. Garofalo, M. Gandolfo, P.L. Baljon, A. Maccione, S. Martinoia, M. Chiappalone, Investigating neuronal activity by SPYCODE multi-channel data analyzer, Neural Netw. 23 (2010) 685–697, doi:10.1016/j.neunet.2010.05.002.
[53] A. Maccione, M. Gandolfo, P. Massobrio, A. Novellino, S. Martinoia, M. Chiappalone, A novel algorithm for precise identification of spikes in extracellularly recorded neuronal signals, J. Neurosci. Methods 177 (2009) 241–249, doi:10.1016/j.jneumeth.2008.09.026.
[54] K. Lingenhohl, D.M. Finch, Morphological characterization of rat entorhinal neurons in vivo: soma-dendritic structure and axonal domains, Exp. Brain Res. 84 (1991), doi:10.1007/BF00231762.
[55] I. Basak, G. Nowicki, B. Ruttens, D. Desta, J. Prooth, M. Jose, S. Nagels, H.-G. Boyen, J. D'Haen, M. Buntinx, W. Deferme, Inkjet printing of PEDOT: PSS based conductive patterns for 3D forming applications, Polymers (Basel) 12 (2020) 2915, doi:10.3390/polym12122915.
[56] X. Geng, O. Kwon, J. Jang, Electrospinning of chitosan dissolved in concentrated acetic acid solution, Biomaterials 26 (2005) 5427–5432, doi:10.1016/j.biomaterials.2005.01.066.
[57] T.-Y. Kuo, C.-F. Jhang, C.-M. Lin, T.-Y. Hsien, H.-J. Hsieh, Fabrication and application of coaxial polyvinyl alcohol/chitosan nanofiber membranes, Open Phys. 15 (2017) 1004–1014, doi:10.1515/phys-2017-0125.
[58] E. Álvarez, G. Vázquez, M. Sánchez-Vilas, B. Sanjurjo, J.M. Navaza, Surface tension of organic acids + water binary mixtures from 20°C to 50°C, J. Chem. Eng. Data 42 (1997) 957–960, doi:10.1021/je970025m.
[59] D. R. J.L. Carvalho-de-Souza, J.S. Treger, B. Dang, S.B. Kent, D.R. Pepperberg, F. Bezanilla, Photosensitivity of neurons enabled by cell-targeted gold nanoparticles, Neuron 86 (2015) 207–217, doi:10.1016/j.neuron.2015.02.033.
[60] H. Kang, G.H. Lee, H. Jung, J.W. Lee, Y. Nam, Inkjet-printed biofunctional thermo-plasmonic interfaces for patterned neuromodulation, ACS Nano 12 (2018) 1128–1138, doi:10.1021/acsnano.7b06617.
[61] M. Mattotti, Z. Alvarez, L. Delgado, M.A. Mateos-Timoneda, C. Aparicio, J.A. Planell, S. Alcántara, E. Engel, Differential neuronal and glial behavior on flat and micro patterned chitosan films, Colloids Surf. B Biointerfaces 158 (2017) 569–577, doi:10.1016/j.colsurfb.2017.07.045.
[62] A. Andolfi, H. Jang, S. Martinoia, Y. Nam, Thermoplasmonic Scaffold design for the modulation of neural activity in three-dimensional neuronal cultures, Biochip J (2022) 1–12, doi:10.1007/s13206-022-00082-z.